

Spin-dependent multiple reentrant localization in an antiferromagnetic helix with transverse electric field: Hopping dimerization-free scenario

Sudin Ganguly,^{1,*} Kallol Mondal,^{2,3,†} and Santanu K. Maiti^{4,‡}

¹*Department of Physics, School of Applied Sciences,
University of Science and Technology Meghalaya, Ri-Bhoi-793101, India*

²*School of Physical Sciences, National Institute of Science Education and Research Bhubaneswar, Jatni, Odisha-752050, India*

³*Homi Bhabha National Institute, Training School Complex, Anushaktinagar, Mumbai-400094, India*

⁴*Physics and Applied Mathematics Unit, Indian Statistical Institute,
203 Barrackpore Trunk Road, Kolkata-700108, India*

Reentrant localization (RL), a recently prominent phenomenon, traditionally links to the interplay of staggered correlated disorder and hopping dimerization, as indicated by prior research. Contrary to this paradigm, our present study demonstrates that hopping dimerization is not a pivotal factor in realizing RL. Considering a helical magnetic system with antiferromagnetic ordering, we uncover spin-dependent RL at multiple energy regions, in the *absence* of hopping dimerization. This phenomenon persists even in the thermodynamic limit. The correlated disorder in the form of Aubry-André-Harper model is introduced by applying a transverse electric field to the helical system, circumventing the use of traditional substitutional disorder. Described within a tight-binding framework, present work provides a novel outlook on RL, highlighting the crucial role of electric field, antiferromagnetic ordering, and the helicity of the geometry.

Introduction: The metal-to-insulator transition is an inevitable consequence of disorder. Despite this, the single-particle wave function displays significant distinctions in behavior when exposed to uncorrelated (random) disorder compared to correlated (quasiperiodic) one. In the presence of random disorder, Anderson localization [1, 2] takes place. The scaling theory [3] of Anderson localization predicts that single-particle states in one- and two-dimensional systems will exhibit exponential spatial localization, even when subjected to extremely weak disorder. Consequently, this leads to the absence of a single-particle mobility edge [4] (SPME). However, an energy-dependent mobility edge can exist in three-dimensional systems. In the context of Anderson localization, extensive investigations have been conducted on numerous fascinating systems across various branches of physics [2, 5–10].

In contrast to the uncorrelated disorder, correlated disorder provides the advantage of a sharply-defined critical point for the extended-localized phase transition [11–13], as well as exhibiting fractal eigenmodes [14, 15] and critical behavior [12, 16] in low-dimensional cases. Among the variety of quasiperiodic models [11–21], the Aubry-André-Harper (AAH) model [11, 22] stands out as the most widely recognized and versatile example. The AAH model, akin to Anderson localization, lacks SPME due to the presence of a distinctly defined critical point characterizing the extended-localized phase transition [11–13]. Nonetheless, researchers have explored various generalizations of the standard AAH model to overcome this limitation. These extensions encompass diverse features, such as exponential short-range hopping [23], flat-band networks [24], higher dimensions [25], power-law hopping [26], flux-dependent hopping [27], and nonequilibrium generalized AAH models [28], among others. Furthermore, the feasibility of AAH systems has been

demonstrated through experimental realizations utilizing cold atoms and optical waveguides [29, 30]. These experimental implementations provide crucial platforms for studying the behavior of AAH models in controlled settings, offering valuable opportunities to explore and validate theoretical predictions in the realm of quantum simulation and condensed matter physics.

Conventionally, it is known that once a state is localized, it continues to remain localized even when the disorder strength is increased. However, recent findings have overturned the long-standing belief. Recently, researchers predicted band-selective localization/delocalization transitions in 1D tight-binding chain [31] and a spin chain with antiferromagnetic nearest-neighbor (NN) coupling [32] in the presence of an interpolating AAH-Fibonacci on-site potential modulation. Experimental validation was performed using cavity-polariton devices for the 1D tight-binding chain [31]. Analogous theoretical outcomes emerged in a 1D NN chain, attributed to the interplay between dimerized hopping and staggered on-site AAH disorder [33]. This reappearance of delocalized states from localized ones, as the staggered AAH disorder strength increases, was termed as reentrant localization (RL). The incorporation of the dimerized 1D chain and staggered on-site AAH disorder have resulted in several studies aiming to achieve RL [34–40]. Drawing upon the insights provided in Refs. [33–40], the present study poses a fundamental inquiry: *Does RL arise exclusively from the interplay between hopping dimerization and staggered on-site AAH disorder?*

In the antiferromagnetic helix (AFH), we assume that the neighboring magnetic moments are aligned along $\pm z$ directions, and since in our framework we consider σ_z as diagonal, the full TB Hamiltonian of the AFH can be decoupled as a sum of up and down spin sub-

Hamiltonians [41]. Due to the anti-parallel configuration of successive magnetic moments, the staggered condition in site energies is easily achieved. Moreover, in the presence of the helicity of the geometry, site energies are correlated in the well-known AAH form upon the application of a transverse electric field [41–47]. So, the helicity, AFM ordering and electric field make the system a unique one. In such a system, probably for the first time we explore spin-dependent RL phenomena at multiple energies, completely in the absence of hopping dimerization. The localization behavior is examined by inspecting various aspects, including the single-particle energy spectrum, inverse participation ratio (IPR), participation ratio (PR), and other relevant measures.

The key findings of the present work are: (i) spin-dependent RL occurs in the presence of electric field in AFH, where hopping dimerization is not a key factor, (ii) total of three RLs are observed, and (iii) The three instances of RL are robust as they persist in the thermodynamic limit.

System and theoretical framework: The schematic diagram of the proposed setup is illustrated in Fig. 1. It depicts a right-handed AFH comprising N magnetic sites, where the magnetic moments of successive sites are aligned in opposite directions ($\pm z$). An external electric field of magnitude E_g is applied perpendicular to the helix axis.

In the AFH, each magnetic site n is characterized by a net spin $\langle \mathbf{S}_n \rangle$. The orientation of these spin vectors is described by the polar angle θ_n and the azimuthal angle φ_n . When an incoming electron interacts with these local magnetic moments, the standard spin-moment exchange interaction J is considered. To incorporate this interaction, a spin-dependent scattering (SDS) parameter is introduced at each site n as $\hat{\mathbf{h}}_n = J\langle \mathbf{S}_n \rangle$ [48]. The magnitude of SDS parameter is denoted as $|\hat{\mathbf{h}}|$, assumed to be isotropic, i.e., $\hat{\mathbf{h}}_n = \hat{\mathbf{h}} \forall n$. It is noteworthy that, for the current investigation, interactions between neighboring magnetic moments are neglected and left for future study.

The tight-binding Hamiltonian for the AFH system in the presence of an electric field is expressed as

$$H = \sum_{n=1}^N \mathbf{c}_n^\dagger (\epsilon_n - \hat{\mathbf{h}}_n \cdot \boldsymbol{\sigma}) \mathbf{c}_n + \sum_{n=1}^N \sum_{m=1}^{N-n} (\mathbf{c}_n^\dagger \mathbf{t}_m \mathbf{c}_{n+m} + h.c.), \quad (1)$$

where, \mathbf{c}_n^\dagger , \mathbf{c}_n , ϵ_n , \mathbf{t}_m are the two-component quantities for the spin-1/2 case and they read as

$$\mathbf{c}_n^\dagger = \begin{pmatrix} c_{n\uparrow}^\dagger & c_{n\downarrow}^\dagger \end{pmatrix}, \quad \mathbf{c}_n = \begin{pmatrix} c_{n\uparrow} \\ c_{n\downarrow} \end{pmatrix}, \\ \epsilon_n = \text{diag}(\epsilon_n, \epsilon_n), \quad \mathbf{t}_m = \text{diag}(t_m, t_m). \quad (2)$$

Here $c_{n\alpha}^\dagger$ ($c_{n\alpha}$) are the creation (annihilation) operator at the n th site with spin α ($=\uparrow, \downarrow$). ϵ_n is the on-site potential

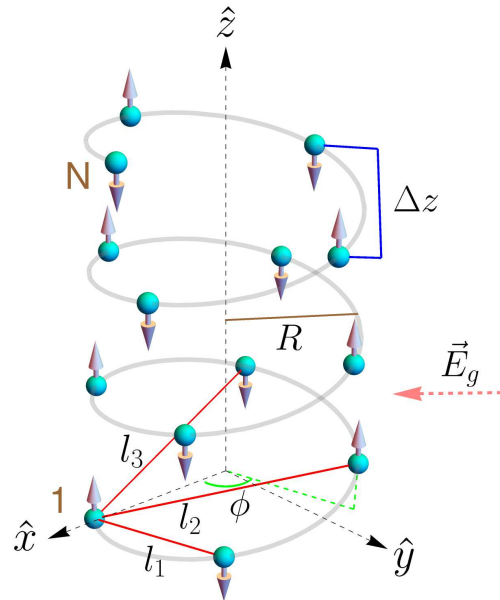


FIG. 1: (Color online). Schematic diagram of an antiferromagnetic right-handed helix. Red balls denote the magnetic sites, where each ball represents a magnetic moment with an arrow indicating its direction. E_g is the electric field, applied perpendicular to the helix axis. l_1 , l_2 , and l_3 are the first, second, and third neighbor distances, respectively. Δz is the stacking distance, the distance along z -axis between two neighboring sites. $\phi = n\Delta\phi$, where $\Delta\phi$ is the twisting angle between the neighboring sites and n is the site index.

at site n and t_m is the hopping integral between the sites n and $n+m$.

In the presence of an external electric field, perpendicular to the helix axis, the site energy modifies as [42]

$$\epsilon_n = eV_g \cos(n\Delta\phi - \beta), \quad (3)$$

where e is the electronic charge and V_g corresponds to the gate voltage associated to the applied electric field E_g with $2V_g = 2E_g R$. β is the angle between the positive x -axis and the incident electric field. Such a modulation of the on-site potential (Eq. 3) can be mapped to the AAH model [11, 22] with a suitable choice of $\Delta\phi$ [44] and thus a correlated disorder can be introduced in the helix with a disorder strength V_g . The inclusion of SDS leads to the effective site energy matrix $(\epsilon_n - \hat{\mathbf{h}}_n \cdot \boldsymbol{\sigma})$, where $\boldsymbol{\sigma}$ is the usual Pauli matrices.

The second term of Eq. 1 is associated with electron hopping in different magnetic sites, where t_m reads as [42, 46]

$$t_m = t e^{-(l_m - l_1)/l_c}. \quad (4)$$

Here l_m is the Euclidean distance between sites n and $n+m$, l_1 and l_c are the nearest-neighbor distance and decay constant, respectively. In terms of radius R (Fig. 1)

of the helix, twisting angle $\Delta\phi$, and stacking distance Δz , l_m takes the form

$$l_m = \sqrt{\left[2R \sin\left(\frac{m\Delta\phi}{2}\right)\right]^2 + [m\Delta z]^2}. \quad (5)$$

To analyze the localization behavior, two commonly used measures are the inverse participation ratio (IPR) and its complementary counterpart, the normalized participation ratio (NPR). For the n th normalized eigenstate, they are defined as [49, 50]

$$\text{IPR}_n = \sum_i |\psi_n^i|^4, \quad \text{NPR}_n = \left(N \sum_i |\psi_n^i|^4\right)^{-1}. \quad (6)$$

In the case of a highly extended state, the IPR approaches to zero, while NPR tends to unity. Conversely, for a strongly localized state, the IPR approximately approaches to unity, and NPR to zero.

The earlier defined IPR_n and NPR_n can be adjusted to characterize the parameter space region where localized and delocalized states coexist, by calculating their averages over a specified subset of states labeled as N_L , defined as [50], and they are

$$\langle \text{IPR} \rangle = \sum_n \frac{\text{IPR}_n}{N_L}, \quad \langle \text{NPR} \rangle = \sum_n \frac{\text{NPR}_n}{N_L}. \quad (7)$$

When all N_L states are localized (delocalized), $\langle \text{IPR} \rangle$ tends to unity (zero) and $\langle \text{NPR} \rangle$ tends to zero (unity). In the parameter range where both $\langle \text{IPR} \rangle$ and $\langle \text{NPR} \rangle$ remain finite, the Hamiltonian's spectrum shows an intermediate phase. Here, spatially extended and localized eigenstates coexist alongside SPME.

Results and Discussion: First, we investigate the spin-resolved IPR characteristics of individual states (defined in Eq. 6), of the AFH in presence of a transverse electric field. For the helical system, the modified on-site energies induced by the electric field can be mapped into a correlated disordered system[42–46, 51]. This mapping effectively relates the modified on-site energies to AAH disorder, with V_g playing the role of the AAH disorder strength. We consider the magnetic moments aligned along the $\pm z$ directions, allowing the Hamiltonian of the AFH to be decoupled into up and down spin components ($H = H_\uparrow + H_\downarrow$). In the absence of an electric field, H_\uparrow and H_\downarrow exhibit symmetry, resulting in zero spin-splitting effect. However, the application of an electric field disrupts this symmetry and a finite mismatch arises between H_\uparrow and H_\downarrow along their respective energy channels [51].

We consider a right-handed helix, characterized by specific structural parameters that render the system a short-range hopping helix. The chosen parameters are radius $R = 8 \text{ \AA}$, stacking distance $\Delta z = 4.3 \text{ \AA}$, twisting angle $\Delta\phi = \pi(\sqrt{5} - 1)/4$, and decay constant $l_c = 0.8 \text{ \AA}$. The selection of $\Delta\phi$ results in on-site energies resembling an incommensurate potential, akin to the AAH disorder.

The number of sites is taken as $N = 1598$ to make the net magnetization zero (N is close to a Fibonacci number 1597). We choose the NNH strength $t = 1 \text{ eV}$ and $\hbar = 0.9$. The direction of the electric field is assumed to be parallel to the positive x -axis, that is $\beta = 0$. It should be noted that the parameter β does not have an impact on the localization properties [31].

It is important to note that as the system size approaches $N \rightarrow \infty$, the values of IPR or NPR for distinct spin species converge, leading to analogous results both for the up-down-spin channels. Therefore, here we concentrate exclusively on the up-spin case, without loss of any generality, and exactly identical scenario will be obtained for the down spin electrons.

As mentioned earlier, the present system Hamiltonian can be separated into up and down spin components. In Fig. 2(a), we depict the energy spectra for the up-spin channels, showcasing the variation with the gate voltage V_g (measured in units of Volts). Each energy point on the plot is assigned a specific color based on its corresponding IPR value, which is calculated according to Eq. 6. To highlight the localization transition, the colorbar employs dark gray to represent the lowest 10% of the maximum IPR values, emphasizing extended states. The remaining portion of the color spectrum ranges from white to dark red, visually representing the increasing degree of local-

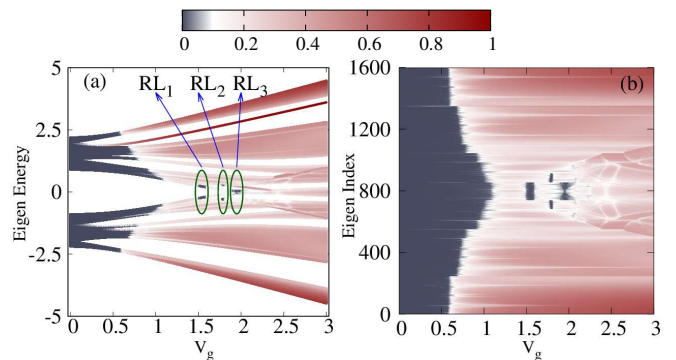


FIG. 2: (Color online). Density plot of IPR for the up spin channel. (a) The energy spectrum vs gate voltage V_g . (b) The energy index vs gate voltage V_g . The color map shows IPR values of different energy eigenstates. $t = 1 \text{ eV}$, $\hbar = 0.9$, $\beta = 0$, and $N = 1598$. The three instances of RL are denoted with RL₁, RL₂, and RL₃ in (a). Their corresponding regions are marked with green ellipses.

ization. Below the threshold of approximately $V_g = 0.5$, nearly all states exhibit an extended nature, as noticed by the dark gray coloration. However, past the point of $V_g \sim 1$, all states undergo a complete localization. The localization persists until around $V_g \sim 1.5$, and subsequently, we identify *three occurrences of RL* from the color-coded IPR values. The three instances of RL are highlighted by green ellipses within the approximate V_g -window: RL₁ from 1.5 to 1.6, RL₂ from 1.78 to 1.8, and RL₃ from 1.9 to 2. A more insightful perspective can be gained by examining the individual eigenstates' IPR, as

shown in Fig. 2(b), where the three instances of RLs are more prominently visible.

To observe the mixed-phase zone, we plot the behavior of $\langle \text{IPR} \rangle$ and $\langle \text{NPR} \rangle$ as a function of V_g as shown in Fig. 3 for the up spin case, represented by the red and green colors, respectively. The averaging for $\langle \text{IPR} \rangle$ and $\langle \text{NPR} \rangle$ is performed over a subset of eigenstates within the range of 30% to 70% of the total states as depicted in Fig. 2(b). All the system and other parameter values remain unchanged with those in Fig. 2. In Fig. 3, both $\langle \text{IPR} \rangle$ and $\langle \text{NPR} \rangle$ become finite for $0.7 > V_g > 1.2$, indicating a critical region with a coexistence of extended and localized states. Beyond $V_g \sim 1.2$, all states become

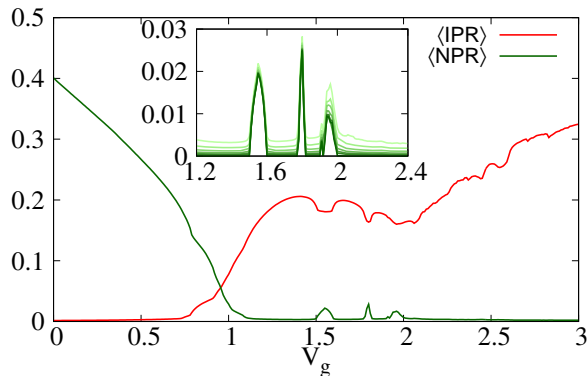


FIG. 3: (Color online). $\langle \text{IPR} \rangle$ (red curve) and $\langle \text{NPR} \rangle$ (green curve) as a function of V_g for a subset of states ranging from 30 to 70% of the eigenstates of Fig. 2(b). All the system parameters remain the same as described in Fig. 2. (Inset) $\langle \text{NPR} \rangle$ versus V_g plot for system sizes $N = 1598, 2584, 4182, 6766, 10946, 17712$ and $N \rightarrow \infty$ represented by light to dark green color.

fully localized. Subsequently, both $\langle \text{IPR} \rangle$ and $\langle \text{NPR} \rangle$ attain finite values in the previously mentioned three RL regions, namely, for $1.5 > V_g > 1.6$, $1.78 > V_g > 1.8$, and $1.9 > V_g > 2$. Therefore, the system hosts as a total of four SPMEs. To mitigate potential finite-size effects, we examine the behavior of $\langle \text{NPR} \rangle$ across various system sizes, specifically, $N = 1598, 2584, 4182, 6766, 10946$, and 17712 . Using the evaluated data, we extrapolate $\langle \text{NPR} \rangle$ as $N \rightarrow \infty$. The corresponding result is presented in the inset of Fig. 3. The same subset of eigenstates as that of the main plot of Fig. 3 is used for the evaluation of $\langle \text{NPR} \rangle$. A gradient of green color, transitioning from light to dark, is employed to represent the behavior of $\langle \text{NPR} \rangle$ as a function of V_g for the system sizes in ascending order. For $N \rightarrow \infty$, $\langle \text{NPR} \rangle$ converges to zero in all the three reentrant localized regions. This clearly demonstrates the robustness of the occurrence of the three RLs with respect to system size and rules out any finite-size effects.

Parameter space: With the confidence that the three RLs are not due to any finite-size effect, we explore the parameter space to identify the conditions under which these three RLs exist. To do so, we compute η , defined

as [52]

$$\eta = \log_{10} [\langle \text{IPR} \rangle \times \langle \text{NPR} \rangle]. \quad (8)$$

In the mixed phase zone, both $\langle \text{IPR} \rangle$ and $\langle \text{NPR} \rangle$ are finite and $\mathcal{O}(1)$, yielding η within $-2 \leq \eta \leq -1$. Conversely, in localized (extended) regime, $\langle \text{NPR} \rangle$ ($\langle \text{IPR} \rangle$) tends toward $\sim N^{-1}$, and $\eta < -\log_{10} N$. For instance, at $N \sim 10^3$, $\eta < -3$. Hence, the quantity η serves as a clear discriminator between fully extended or localized phase and a mixed phase.

First, we explore the behavior of η in the phase space of V_g and \hbar for the up spin channel as shown in Fig. 4(a). All other parameters remain constant as indicated in Fig. 2. In the colorbar of η , steel blue color corresponds to the extended or localized phase, while the brown color represents the mixed phase. In Fig. 4(a), the localized or extended phases are determined by analyzing the $\langle \text{IPR} \rangle$ and $\langle \text{NPR} \rangle$ values. All three RLs emerge within the \hbar -range of approximately 0.75 to 0.96. The third RL ceases to exist beyond $\hbar \sim 0.96$. Additionally, no instances of RL are present beyond $\hbar \sim 1.2$. This observation strongly suggests that RL occurrence is possible when \hbar is comparable to the numerical value of V_g .

Second, we study the η -behavior in the phase space of V_g and t for the up spin channel as shown in Fig. 4(b). All other parameters kept unchanged as indicated in Fig. 2. As both V_g and t increase from zero to a finite value, the width of the first critical region expands. The first RL emerges around $t \sim 0.8$. The second RL becomes noticeable around $t \sim 0.9$, and the third one around $t \sim 1$. The first RL diminishes beyond $t \sim 1.1$, the second one around $t \sim 1.15$, and the third one for $t \sim 1.25$. All three RLs are pronounced within the range of approximately $1 < t < 1.1$. This range is comparable to the numerical value of \hbar , which is fixed at $\hbar = 0.9$, consistent with the previous analysis. After $t \sim 1.25$, all RLs vanish and merge into the first critical region.

So far, all the results were discussed for the scenario of short-range hopping. To investigate the transition from short-range hopping to long-range hopping and understand the localization behavior, we examine the η -behavior within the V_g and l_c phase space, as illustrated in Fig 4(c). The variation of the decay constant spans from 0.1 \AA to 8.5 \AA , thereby inducing a shift from a short-range hopping regime to a long-range hopping scenario. In accordance with Fig. 2, the remaining parameters are maintained at their specified values without any alterations. For low values of l_c (primarily SRH) within the range of 0.1 to 2 \AA , the V_g -window associated with the first critical region remains nearly constant and it expands as l_c increases. The three RLs are present right from $l_c = 0.1 \text{ \AA}$. The first RL converges with the first critical region at approximately $l_c \sim 0.75 \text{ \AA}$, but the second and third RLs persist with increasing l_c . The second RL unites with the first critical region while the third one survives till $l_c \sim 4 \text{ \AA}$. Ultimately, the third RL disappears at approximately $l_c \sim 5 \text{ \AA}$, leaving only one critical

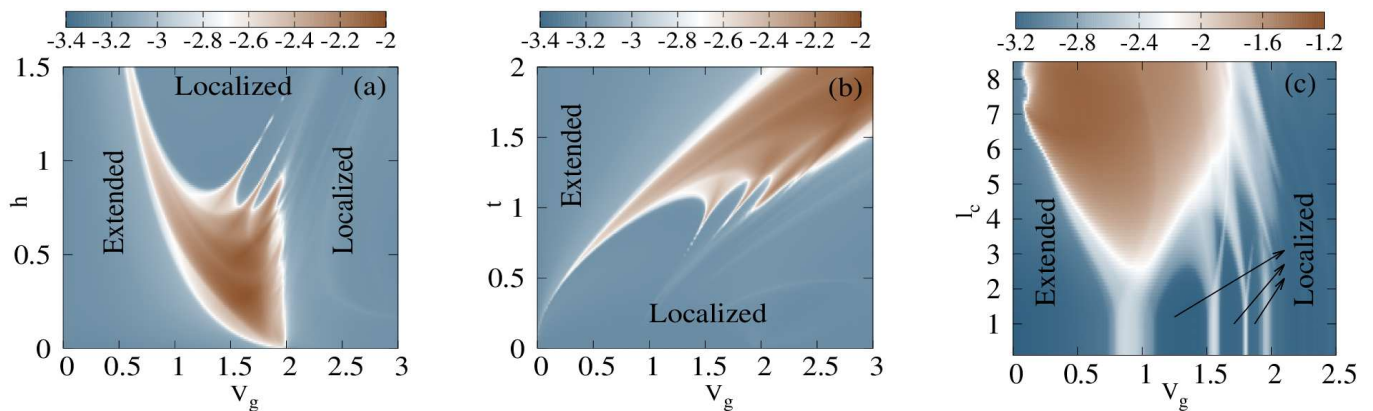


FIG. 4: (Color online). Density plot of η in the (a) V_g - h , (b) V_g - t , and (c) V_g - l_c planes. The system size and all the other parameters remain the same as described in Fig. 2.

region beyond that point. Another notable observation is that from the first RL, a secondary RL emerges within a brief V_g window with l_c between 3 to 4 Å, and subsequently integrates with the second RL. A similar scenario is observed for the second RL, wherein another secondary RL originates from $l_c \sim 2$ Å and then dissipates into the localized region beyond $l_c \sim 3$ Å.

Conclusion: The present investigation has revealed the occurrence of multiple spin-dependent reentrant localization in a helical system when subjected to an electric field with net zero magnetization, characterized by antiferromagnetic ordering of the moments. Crucially, this accomplishment has been realized without incorporating any hopping dimerization scenario, a factor upon which previous studies attributing the occurrence of RL had relied. Our study of spin-resolved IPR values across various energy states has revealed the presence of three distinct RLs. The robustness of these three RLs has been affirmed through a comprehensive analysis of averaged IPR and NPR values in the limit as the system size approaches infinity ($N \rightarrow \infty$). The investigation of η -behavior unravels that RL become apparent when the electric field strength V_g is on a comparable scale to the value of \hbar . Additionally, in the V_g - l_c plane, it is notable that RLs vanish as the system transitions from the short-range hopping to the long-range hopping case. Furthermore, our investigation has identified two secondary RLs stemming from the first and second RLs, which however warrants further in-depth exploration.

Overall, exploring the practical implications of spin-dependent reentrant localization without hopping dimerization could lead to innovative applications in quantum technologies. Further, investigating the behavior of RL in the V_g - l_c plane holds promise for understanding and controlling localization phenomena in helical systems, as the system undergoes systematically from a short-range hopping to a long-range hopping regime.

* Electronic address: sudinganguly@gmail.com

† Electronic address: kallolsankarmondal@gmail.com

‡ Electronic address: santanu.maiti@isical.ac.in

- [1] P. W. Anderson, *Absence of diffusion in certain random lattices*, Phys. Rev. **109**, 1492 (1958).
- [2] P. A. Lee and T. V. Ramakrishnan, *Disordered electronic systems*, Rev. Mod. Phys. **57**, 287 (1985).
- [3] E. Abrahams, P. W. Anderson, D. C. Licciardello, and T. V. Ramakrishnan, *Scaling Theory of Localization: Absence of Quantum Diffusion in Two Dimensions*, Phys. Rev. Lett. **42**, 673 (1979).
- [4] N. Mott, *The mobility edge since 1967*, J. Phys. C **20**, 3075 (1987).
- [5] B. Kramer and A. MacKinnon, *Localization: theory and experiment*, Rep. Prog. Phys. **56**, 1469 (1993).
- [6] D. S. Wiersma, P. Bartolini, A. Lagendijk, and R. Righini, *Localization of light in a disordered medium*, Nature **390**, 671 (1997).
- [7] T. Schwartz, G. Bartal, S. Fishman, and M. Segev, *Transport and Anderson localization in disordered two-dimensional photonic lattices*, Nature **446**, 52 (2007).
- [8] H. Hu, A. Strybulevych, J. H. Page, S. E. Skipetrov, and B. A. van Tiggelen, *Localization of ultrasound in a three-dimensional elastic network*, Nat. Phys. **4**, 945 (2008).
- [9] W. R. McGehee, S. S. Kondov, W. Xu, J. J. Zirbel, and B. DeMarco, *Three-Dimensional Anderson Localization in Variable Scale Disorder*, Phys. Rev. Lett. **111**, 145303 (2013).
- [10] M. Segev, Y. Silberberg, and D. N. Christodoulides, *Anderson localization of light*, Nature Photon **7**, 197 (2013).
- [11] S. Aubry and G. André, *Analyticity breaking and Anderson localization in incommensurate lattices*, Ann. Isr. Phys. Soc. **3**, 133 (1980).
- [12] S. Y. Jitomirskaya, *Metal-insulator transition for the almost Mathieu operator*, Ann. Math. **150**, 1159 (1999).
- [13] C. Aulbach, A. Wobst, G.-L. Ingold, P. Hänggi, and I. Varga, *Phase-space visualization of a metal-insulator transition*, New J. Phys. **6**, 70 (2004).
- [14] M. Kohmoto, L. P. Kadanoff, and C. Tang, *Localization problem in one dimension: mapping and escape*, Phys. Rev. Lett. **50**, 1870 (1983).
- [15] S. Ostlund, R. Pandit, D. Rand, H. J. Schellnhuber, and E. D. Siggia, *One-dimensional Schrödinger equation with*

- an almost periodic potential, Phys. Rev. Lett. **50**, 1873 (1983).
- [16] J.-B. Suck, M. Schreiber, and P. Häussler, *Quasicrystals: An Introduction to Structure, Physical Properties and Applications*, Vol. 55 (Springer, 2013).
- [17] F. A. B. F. de Moura and M. L. Lyra, *Delocalization in the 1D Anderson model with long-range correlated disorder*, Phys. Rev. Lett. **81**, 3735 (1998).
- [18] F. M. Izrailev and A. A. Krokhin, *Localization and the Mobility Edge in One-Dimensional Potentials with Correlated Disorder*, Phys. Rev. Lett. **82**, 4062 (1999).
- [19] P. Carpena, P. Bernaola-Galván, P. C. Ivanov, and H. E. Stanley, *Metal-insulator transition in chains with correlated disorder*, Nature **418**, 955 (2002).
- [20] F. M. Izrailev, A. A. Krokhin, and N. M. Makarov, *Anomalous localization in low-dimensional systems with correlated disorder*, Phys. Rep. **512**, 125 (2012).
- [21] G. M. Conley, M. Burrelli, F. Pratesi, K. Vynck, and D. S. Wiersma, *Localization and the mobility edge in one-dimensional potentials with correlated disorder*, Phys. Rev. Lett. **112**, 143901 (2014).
- [22] P. G. Harper, *The general motion of conduction electrons in a uniform magnetic field, with application to the diamagnetism of metals*, Proc. R. Soc. London, Ser. A **68**, 874 (1955).
- [23] J. Biddle and S. Das Sarma, *Predicted Mobility Edges in One-Dimensional Incommensurate Optical Lattices: An Exactly Solvable Model of Anderson Localization*, Phys. Rev. Lett. **104**, 070601 (2010).
- [24] C. Danieli, J. D. Bodyfelt, and S. Flach, *Flatband engineering of mobility edges*, Phys. Rev. B **91**, 235134 (2015).
- [25] T. Devakul and D. A. Huse, *Anderson localization transitions with and without random potentials*, Phys. Rev. B **96**, 214201 (2017).
- [26] S. Gopalakrishnan, *Self-dual quasiperiodic systems with power-law hopping*, Phys. Rev. B **96**, 054202 (2017).
- [27] F. A. An, R. J. Meier, and B. Gadway, *Engineering a Flux-Dependent Mobility Edge in Disordered Zigzag Chains*, Phys. Rev. X **8**, 031045 (2018).
- [28] A. Purkayastha, A. Dhar, and M. Kulkarni, *Nonequilibrium phase diagram of a one-dimensional quasiperiodic system with a single-particle mobility edge*, Phys. Rev. B **96**, 180204(R) (2017).
- [29] Y. E. Kraus, Y. Lahini, Z. Ringel, M. Verbin, and O. Zeitler, *Topological States and Adiabatic Pumping in Quasicrystals*, Phys. Rev. Lett. **109**, 106402 (2012).
- [30] M. Lohse, C. Schweizer, H. M. Price, O. Zeitler, and I. Bloch, *Exploring 4D quantum Hall physics with a 2D topological charge pump*, Nature (London) **553**, 55 (2018).
- [31] V. Goblot et al, *Emergence of criticality through a cascade of delocalization transitions in quasiperiodic chains*, Nat. Phys. **16**, 832 (2020).
- [32] A. Štrkalj, E. V. H. Doggen, I. V. Gornyi, and O. Zeitler, *Many-body localization in the interpolating Aubry-André-Fibonacci model*, Phys. Rev. Research **3**, 033257 (2021).
- [33] S. Roy, T. Mishra, B. Tanatar, and S. Basu, *Reentrant Localization Transition in a Quasiperiodic Chain*, Phys. Rev. Lett. **126**, 106803 (2021).
- [34] C. Wu, J. Fan, G. Chen, and S. Jia, *Non-Hermiticity-induced reentrant localization in a quasiperiodic lattice*, New J. Phys. **23**, 123048 (2021).
- [35] X.-P. Jiang, Y. Qiao, and J.-P. Cao, *Mobility edges and reentrant localization in one-dimensional dimerized non-Hermitian quasiperiodic lattice*, Chin. Phys. B **30**, 097202 (2021).
- [36] Z.-W. Zuo and D. Kang, *Reentrant localization transition in the Su-Schrieffer-Heeger model with random-dimer disorder*, Phys. Rev. A **106**, 013305 (2022).
- [37] A. Padhan, M. K. Giri, S. Mondal, and T. Mishra, *Emergence of multiple localization transitions in a one-dimensional quasiperiodic lattice*, Phys. Rev. B **105**, L220201 (2022).
- [38] H. Wang, X. Zheng, J. Chen, L. Xiao, S. Jia, and L. Zhang, *Fate of the reentrant localization phenomenon in the one-dimensional dimerized quasiperiodic chain with long-range hopping*, Phys. Rev. B **107**, 075128 (2023).
- [39] S.-Z. Li and Z. Li, *The multiple re-entrant localization in a phase-shift quasiperiodic chain*, arXiv:2305.12321 (2023).
- [40] S. Aditya, K. Sengupta, and D. Sen, *Periodically driven model with quasiperiodic potential and staggered hopping amplitudes: Engineering of mobility gaps and multifractal states*, Phys. Rev. B **107**, 035402 (2023).
- [41] D. D. Gupta and S. K. Maiti, *Antiferromagnetic helix as an efficient spin polarizer: Interplay between electric field and higher-order hopping*, Phys. Rev. B **106**, 125420 (2022).
- [42] A. V. Malyshev, *DNA Double Helices for Single Molecule Electronics*, Phys. Rev. Lett. **98**, 096801 (2007).
- [43] A.-M. Guo and Q.-F. Sun, *Enhanced spin-polarized transport through DNA double helix by gate voltage*, Phys. Rev. B **86**, 035424 (2012).
- [44] S. Sarkar and S. K. Maiti, *Localization to delocalization transition in a double stranded helical geometry: Effects of conformation, transverse electric field and dynamics*, Phys. Rev. B **100**, 205402 (2019).
- [45] T.-R. Pan, A.-M. Guo, and Q.-F. Sun, *Effect of gate voltage on spin transport along α -helical protein*, Phys. Rev. B **92**, 115418 (2015).
- [46] A.-M. Guo and Q.-F. Sun, *Topological states and quantized current in helical organic molecules*, Phys. Rev. B **95**, 155411 (2017).
- [47] A.-M. Guo and Q.-F. Sun, *Spin-dependent electron transport in protein-like single-helical molecules*, Proc. Natl Acad. Sci. USA **111**, 11658 (2014).
- [48] Y.-H. Su, S.-H. Chen, C. D. Hu, and C.-R. Chang, *Competition between spin-orbit interaction and exchange coupling within a honeycomb lattice ribbon*, J. Phys. D: Appl. Phys. **49**, 015305 (2015).
- [49] X. Li, X. Li, and S. D. Sarma, *Mobility edges in one-dimensional bichromatic incommensurate potential*, Phys. Rev. B **96**, 085119 (2017).
- [50] M. Rossignolo and L. Dell'Anna, *Localization transitions and mobility edges in coupled Aubry-André chains*, Phys. Rev. B **99**, 054211 (2019).
- [51] K. Mondal, S. Ganguly, and S. K. Maiti, *Thermoelectric phenomena in an antiferromagnetic helix: Role of electric field*, Phys. Rev. B **108**, 195401 (2023).
- [52] X. Li and S. D. Sarma, *Mobility edge and intermediate phase in one-dimensional incommensurate lattice potentials*, Phys. Rev. B **101**, 064203 (2020).